Temperature evolution in IR action spectroscopy experiments with sodium doped water clusters

Daniel Becker[a], Christoph W. Dierking[a,‡], Jiri Suchan[b], Florian Zurheide[a], Jozef Lengyel[c], Michal Fárník[d], Petr Slavíček[b], Udo Buck[e], and Thomas Zeuch[a*]

[a] *Universität Göttingen, Institut für Physikalische Chemie, Tammanstr. 6, 37077 Göttingen, Germany. *E-mail: tzeuch1@gwdg.de*

[b] *Department of Physical Chemistry, University of Chemistry and Technology, Technická 5, Prague 6, Czech Republic*

[c] *Lehrstuhl für Physikalische Chemie, Technische Universität München, Lichtenbergstr.4, 85748, Garching, Germany*

[d] *J. Heyrovsky Institute of Physical Chemistry, v.v.i., Academy of Sciences of the Czech Republic, Doljškova 3, 182 23 Prague 8, Czech Republic*

[e] *Max-Planck Institut für Dynamik und Selbstorganisation, Am Faßberg 17, 37077 Göttingen, Germany*

[‡] *Now at Lonza Solutions AG, 3930 Visp, Switzerland*

1 Temperature dependence of $Na(H_2O)_n$ spectra for $n = 2, 3$

In the main manuscript, we discuss the temperature dependence of ionization spectra for the case of $n = 7$. We have also simulated a set of smaller clusters ($n = 2, 3$) with identical simulation parameters. The results (figure S1 and figure S2) confirm the clear trend of temperature dependence. The results for 400 K were discarded because of heavy water evaporation from the cluster at this temperature.

Simulation details: D2-LC-wPBE/6-31++g** method, time step 0.5 fs, swaps attempted every 50 steps, NH thermostat. The total runtime of simulations was 350 fs for $n = 2$ and 430 fs for $n = 3$. The ionization energies were calculated every 1000th geometry at the BMK/6-31++g** level, broadening parameter was set to 0.05 eV.

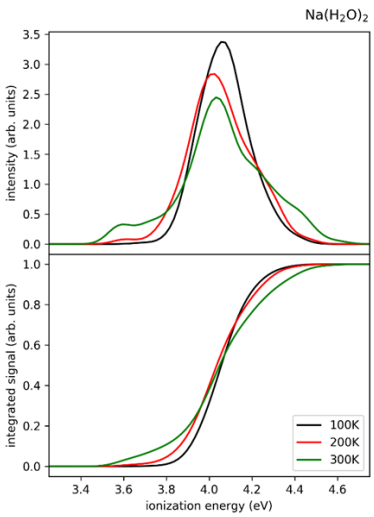

Figure S1: Simulated ionization curves at different cluster temperatures for $(H_2O)_2$.

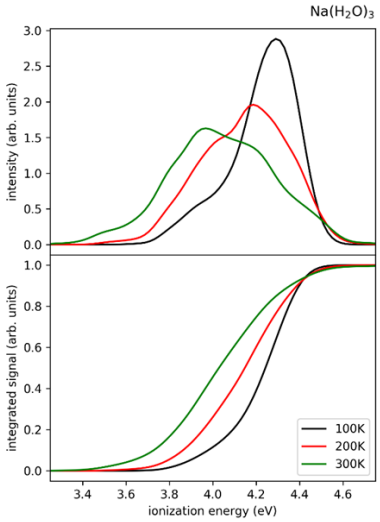

Figure S2: Simulated ionization curves at different cluster temperatures for $(H_2O)_3$.

2 Experimental Equipment and Materials

The molecular beam apparaturs has been described in detail elsewhere.[1] Clusters were generated in a conical nozzle with $\bar{d} \approx 75\,\mu m$ using purified water (bidest.) and high purity gases (He $\geq$ 99.996%, Ar$\geq$ 99.999%).

For IR-excitation of the clusters we used a tunable OPO/OPA (Laservision) pumped by a Powerlite Precision II 8000 (Continuum). Photoionization was achieved *via* a dye laser (Sirah Cobra Stretch) operated at 385 nm and pumped with the third harmonic of a Nd:YAG-laser (Continuum Powerlite DSL 9010). Typical pulse energies are $\approx 10.5\,mJ$ for the IR- and $\approx 5\,mJ$ for the UV pulse. Pulse width was in the range of $\approx 10\,ns$ and the delay between both pulses was set by a delay generator (DG535 , Stanford Research Systems Inc.). The delay was calibrated using a photodiode (Electro Optics Technology, Inc., Model Silicon PIN Detector ET-2000) and an oscilloscope (Tektronix TDS 2004B) with an estimated uncertainty of $\approx 2\,ns$.

Each cluster size distribution shown in Fig. 4 (main text) originates from 9000 to 13000 added mass spectra, which were rebinned, normalized and smoothed once by a Savitzky-Golay-Filter for sake of clarity.
The delay traces in Fig. 7 (main text) are based on 10000 ($3200\,cm^{-1}$) and 13000 ($3400\,cm^{-1}$) summed up mass spectra with typical energies of $\approx 10.2\,mJ$ (IR) and $\approx 4.2\,mJ$ (UV). The ratio of integrated ion yield in the cluster range $n = 300 - 400$ was calculated and an offset of 1 was subtracted, giving the ion signal change as a function of delay time.

Processing of experimental mass spectra was realized with Python (ver. 3.4).[2]

3 Kinetic Simulation

Here, we present our preliminary kinetic model for evaporation describing the overall process as a series of successive monomer evaporation (see equation S1). The following concepts are similar to work reported by the group of HANSEN.[3] N_0 is the number of initial clusters having temeperature T_{c0} and size n_0. Every pair of T, n represents a point in phase space and inital clusters follow a trajectory through that space. This trajectory is determenistic, because we exclude rethermalization by collisions with gases and other clusters, since the relative velocities in the molecular beam are approximately zero at this point.[4] Since a broad cluster distribution emerges from the nozzle, many intial states and therefore individual trajectories have to be considered.

$$N_0(T_{c0}, n_0) \xrightarrow{k(T_{c0},n_0)} N_1(T_{c1}, n_1) \xrightarrow{k(T_{c1},n_1)} \dots \xrightarrow{k(T_{cj-1},n_{j-1})} N_j(T_{cj}, n_j) \quad \text{(S1)}$$

The basic idea of our model is to use a two dimensional matrix as reprentation for phase space, where a matrix element $a_{T_c,n}$ is a bin of certain temperature and size cointaining N clusters (see figure S3). This allows an easy implementation in Python (ver. 3.7) providing suitible tools for matrix operations. In this study, temperature intervals were set to 0.1 K and size intervals to 1 monomer.

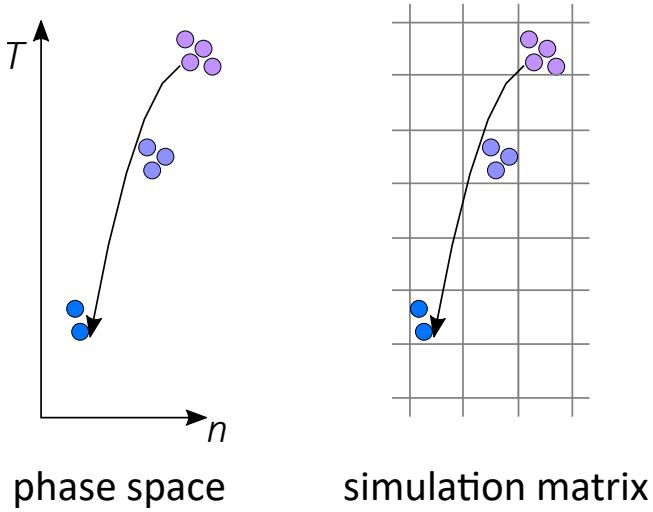

Figure S3: Schematic trajectory of clusters through phase space represented by a matrix. Cluster size and temperature (color coding) decrease.

Prior to the simulation loop we calculated the size- and temperature-dependent rate coefficients $k(n, T_c)$ stored in the "k matrix". We use a description from BORNER *et al.*[5], shown in equation S2, with $E_{\text{bin}} = 6.255 \times 10^{-20}\,\text{kJ}\,\text{mol}^{-1}$ and a prefacor of $\omega = 2.68 \times 10^{12}\,\text{s}^{-1}$. However, there are other descriptions of the rate coefficients in the literature[6–9], so that this is a major uncertainty and

needs further evaluation.

$$k(n, T_c) = n^{2/3} \omega \exp\left(\frac{-E_{\mathrm{bin}}}{k_{\mathrm{B}} T}\right) \tag{S2}$$

The cluster heat capacities $C_c(n, T_c)$ were calculated according to equation S3. Gimelshein *et al.*[10] showed, that the heat capacity per monomer is constant for clusters with $n \geq 14$. Temperature dependence is not included yet, but simulations from Borner *et al.* indicate only a minor dependence for clusters with $n = 10$ for a range of 100 K.[5] Of course, phase transitions e.g. crystallisation of clusters would change the value, as was shown from experiments by Hock *et al.*[11] and thus, implementing the temperature-dependence is subject to further investigation.

$$\frac{C_c(n)}{n} = 8.1 k_{\mathrm{B}} \tag{S3}$$

It is assumed that evaporation of one monomer removes the energy E_{bin} from the cluster, so that the temperature change can be calculated as:

$$C_c(n) = \frac{\mathrm{d}U}{\mathrm{d}T_c} \approx \frac{E_{\mathrm{bin}}}{\Delta T_c} \Rightarrow \Delta T_c = \frac{E_{\mathrm{bin}}}{C_c(n)} \tag{S4}$$

The last missing step is to fill the bins with clusters. For this the experimental cluster distribution without IR-irradiation is interpreted as an alias for an irradiated cluster distribution at $t = 0$ ns and is loaded into the matrix, in which the initial temperature is taken from an input file. During a timestep of $\Delta t = 1$ ns the fraction of evaporating species is calculated according to:

$$\Delta N(n, T_c) = k(n, T_c) \cdot N(n, t) \cdot \Delta t \tag{S5}$$

Doing this for all clusters in different bins is achieved by elementwise multiplication of simulation matrix and the k-matrix.The fraction of evaporated species is subtracted from the original bin and added to the new bin, for which we employ a mapping sheme calculated at the beginning of the loop.
Finally, the average temperature of cluster with size n is calculated, using the population of bins as weighting factor. Additionally, all clusters of the same size are summed yielding the altered distribution. As shown in figure S4 a monodispers distribution of clusters with $n = 100$ leads to broadened distributions of smaller clusters. We can use this distributions as weightings for a second averaging over the averaged temperatures in each bin. So all clusters are taken into account and therefore the cooling of the intial clusters can be followed (see Fig. 6 in main text)

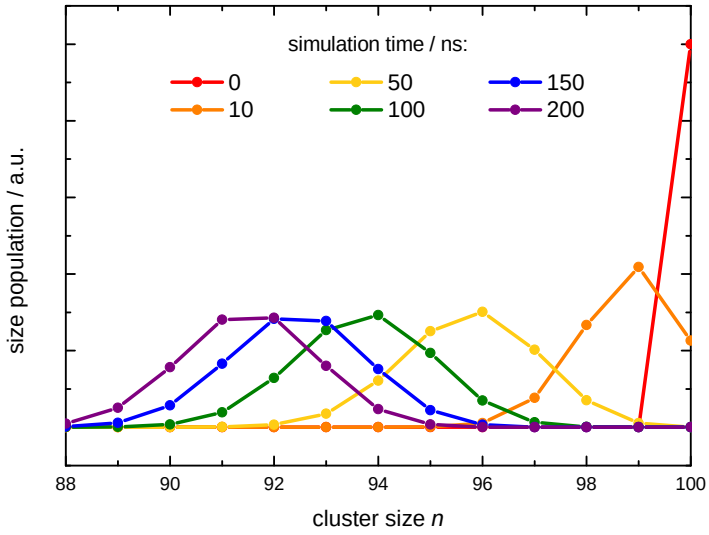

Figure S4: Evaporation of monodipers distribution with $n = 100$ and initial temperature of 350 K at different simulation times. The populaion in this transient distributions $N(n,t)$ as used as weighting factor for the averaged temperature $\bar{T}(n,t)$.

4 Ion Signal Change on long time scale

According to figure 7 in the main text we show the temporal dependence of the IR signal gain in figure S5 and can identify four time domains.[12] For negative delay times clusters are ionized first and heated up afterwards. Contrastingly to figure 7 (main text) we observe a small positiv signal change instead of a loss. This is because the population of $n = 100$–200 is a convolution of evaporation loss of $n = 100$–200 and gain from clusters with $n > 200$.
At delay times up to $\Delta t \approx 10$ ns both laser pulses are overlapping and a sharp signal gain is observed as the consequence of the enhanced abundace of warm clusters with low ionization energies.
Enlarging the temporal gap between IR excitation und photoionization is observed in the third section. Due to evaporative cooling the abundance of warm clusters decreases and so does the IR-induced ion signal gain.
For very large delay times a second decrease of ion signal change can be seen which is not exponential but linear (at least at the beginning). We attribute this finding to the flyout of IR-irradiated clusters beyond the volume probed by the ionizing laser pulse.

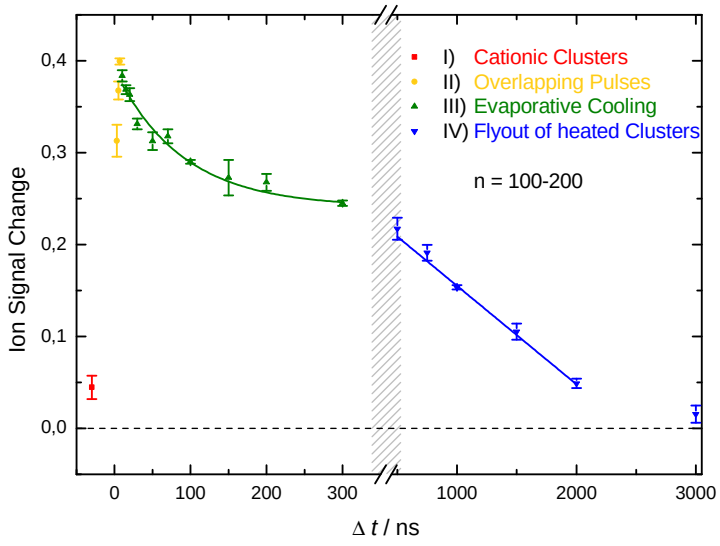

Figure S5: Delay time dependence of the IR signal at 3400 cm^{-1} integrated from $n = 100$–200. The experimental conditions are those of the helium experiment mentioned in the main text. Here, we the UV-wavelength was 355 nm.

References

[1] S. Schütte, U. Buck, "Strong fragmentation of large rare gas clusters by high energy electron impact", *International Journal of Mass Spectrometry* **2002**, *220*, 183–192, DOI 10.1016/s1387-3806(02)00670-x.

[2] F. Zurheide, PhD thesis, Georg-August-University Göttingen, **2020**.

[3] U. Näher, K. Hansen, "Temperature of large clusters", *The Journal of Chemical Physics* **1994**, *101*, 5367–5371, DOI 10.1063/1.467390.

[4] D. R. Moberg, D. Becker, C. W. Dierking, F. Zurheide, B. Bandow, U. Buck, A. Hudait, V. Molinero, F. Paesani, T. Zeuch, "The end of ice I", *Proceedings of the National Academy of Sciences* **2019**, *116*, 24413–24419, DOI 10.1073/pnas.1914254116.

[5] A. Borner, Z. Li, D. A. Levin, "Development of a molecular-dynamics-based cluster-heat-capacity model for study of homogeneous condensation in supersonic water-vapor expansions", *The Journal of Chemical Physics* **2013**, *138*, 064302, DOI 10.1063/1.4790476.

[6] C. Caleman, D. van der Spoel, "Temperature and structural changes of water clusters in vacuum due to evaporation", *The Journal of Chemical Physics* **2006**, *125*, 154508, DOI 10.1063/1.2357591.

[7] Y. Okada, Y. Hara, "Calculation of the Sticking Probability of a Water Molecule to a Water Cluster", *Earozoru Kenkyu* **2007**, *22*, 147–151, DOI 10.11203/jar.22.147.

[8] F. Calvo, J. Douady, F. Spiegelman, "Accurate evaporation rates of pure and doped water clusters in vacuum: A statistico-dynamical approach", *The Journal of Chemical Physics* **2010**, *132*, 024305, DOI 10.1063/1.3280168.

[9] R. Jansen, N. Gimelshein, S. Gimelshein, I. Wysong, "A Lagrangian–Eulerian approach to modeling homogeneous condensation in high density gas expansions", *The Journal of Chemical Physics* **2011**, *134*, 104105, DOI 10.1063/1.3562370.

[10] N. Gimelshein, S. Gimelshein, C. C. Pradzynski, T. Zeuch, U. Buck, "The temperature and size distribution of large water clusters from a non-equilibrium model", *The Journal of Chemical Physics* **2015**, *142*, 244305, DOI 10.1063/1.4922312.

[11] C. Hock, M. Schmidt, R. Kuhnen, C. Bartels, L. Ma, H. Haberland, B. v.Issendorff, "Calorimetric Observation of the Melting of Free Water Nanoparticles at Cryogenic Temperatures", *Physical Review Letters* **2009**, *103*, DOI 10.1103/physrevlett.103.073401.

[12] C. W. Dierking, PhD thesis, Georg-August-University Göttingen, **2019**.